NRIAG JOURNAL OF ASTRONOMY AND GEOPHYSICS
2020, VOL. 9, NO. 1, 155–167
https://doi.org/10.1080/20909977.2020.1728893



# Airborne gamma-ray spectrometric data interpretation on Wadi Queih and Wadi Safaga area, Central Eastern Desert, Egypt

Reda A. Y. El Qassas[a], M Salaheldin[b], S.M. Assran Assran[a], Th. Abdel Fattah[b] and M.A. Rashed[b]

[a]Exploration Division, Nuclear Materials Authority, Cairo, Egypt; [b]Geology Department, Faculty of Science, Alexandria University, Alexandria, Egypt

**ABSTRACT**
Wadi Queih and Wadi Safaga lie in the central part of the Eastern Desert of Egypt. The airborne gamma-ray spectrometric data of the study area have been interpreted qualitatively and quantitatively and correlated with the surface lithologic units to define the anomalous uranium zones and to reveal if any association is present between the radiometric anomalies and the structural trends.The radiometric data have been treated statistically. The results revealed that the area has a wide range of radioactivity ranging from 0.1 to 23.6 Ur for the total-count (TC), 0.1 to 3.3 % for potassium (K), 0.01 to 19.1 ppm for equivalent uranium (eU), and 0.29 to 18.9 ppm for equivalent thorium (eTh). The calculated CV values for all the rock units in the study area are less than 100% for three radio-elements (K, eU, eTh), except for potassium in Thebes Formation. The younger granites and Duwi Formation have the highest radiometric values. The lowest values exist over ophiolitic metagabbro, basic metavolcanics, metasediments, serpentinites, and Umm Gheig Formation. The generated composite radio-elements and composite image maps define the locations of the high anomalous radiometric and eU zones as bright white areas. The most radioactive anomalies have NW-SE and NE-SW trends.

**ARTICLE HISTORY**
Received 10 August 2019
Revised 30 December 2019
Accepted 15 January 2020

**KEYWORDS**
Spectrometric; interpretation; Eastern Desert; Wadi Quieh; Wadi Safaga

## 1. Introduction

Wadi Queih and wadi Safaga lie in the Central Eastern Desert of Egypt between Latitudes 26° 16′ 06″ N & 26° 37′ 00″ N and Longitudes 33° 37′ 20″ E & 34° 01′ 00″ E (Figure 1). Different Terrains exist and vary from gentle to rough topography (Figure 2). A wide diversity of igneous, metamorphic and sedimentary rocks ranging in age from Precambrian to Quaternary is recognised in the study area. Several wadies (dry valleys), filled with alluvial sediments traverse these rocks. The airborne gamma-ray spectrometric survey was conducted by Aero-Service Division, Western Geophysical Company of America over a large segment of the central and south Eastern Desert of Egypt, with a flight altitude of 120 m. terrain clearance, 1 km. flight line interval and 10 km tie line spacing carried out the radiometric survey (Aero-Service 1984).

The radioactivity is related to the presence of natural radio-elements (U, Th, and K40), which vary measurably and significantly with lithology (Darnely and Ford 1989). Thus, the surface and near-surface features as derived from the surface geologic map can be correlated well with the analysis of the radiometric maps. Environmental studies, geological mapping, and mineral exploration use the gamma-ray spectrometric survey IAEA, 2003). The aim of the current study is to identify the anomalous uranium zones and to reveal if any association is present between both the structural trends and uranium anomalies in the study area.

## 2. Geologic setting

Based on the geological map of Quseir quadrangle, Egypt, at a scale of 1:500000 (Conoco and EGPC, 1987), the geology of the study area has observed. It comprises a wide diversity of igneous, metamorphic, and sedimentary rocks ranging in age from Precambrian to Quaternary (Figure 3).

The Pre-Cambrian basement rocks of the Eastern Desert of Egypt have been distinguished and classified by Hume (1937), Ibrahim (1941), Akaad and El-Ramly (1960b) and El-Ramly (1972). The Pre-Cambrian rocks constitute about 70% of the study area (Figure 3). The main Precambrian basement rock units in the study area arranged from the oldest to the youngest as serpentinite, metagabbro-diorite complex, ophiolitic metagabbro, metavolcanics, metasediments, Hammamat sediments, gabbroic rocks, older granites, younger granites, Dokhan volcanic and post-Hammamat felsite.

The age of the sedimentary rocks in the study area ranges from Cretaceous to Quaternary. They overlie the Precambrian basement rocks unconformably and comprises several formations arranged from the oldest as,

**CONTACT** M Salaheldin mohamed.salaheldin1089@gmail.com Geology DepartmentFaculty of Science, Alexandria University,Alexandria, Egypt

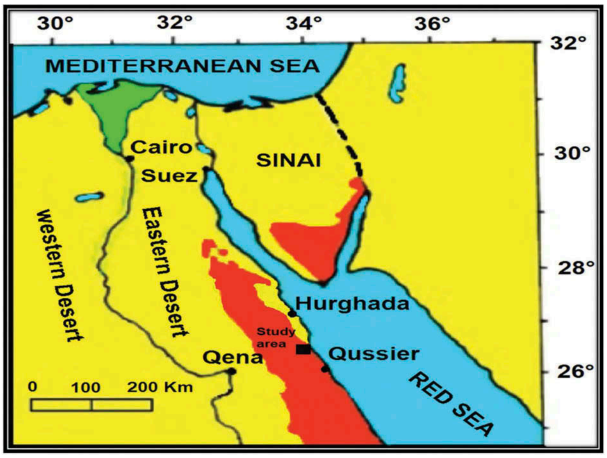


**Figure 1.** Location map of the study area, Central Eastern Desert, Egypt.

Taref Formation, Duwi Formation, Dakhla Formation, Tarwan Formation, Esna Formation, Thebes Formation, Nakheil Formation, Umm Mahara Formation, Umm Gheig Formation, and Shagra Formation. The most important of these sedimentary formations is Duwi Formation, which consists of phosphate beds alternating with black shale, marl, and Oyster limestone. The phosphate deposits were subjected to many geological and radiometric investigations, which showed that phosphates contain economic concentrations of uranium (Sadek 1972; Salman 1974; Ammar et al. 1988; Salahel-Din 2009; El Qassas (2018)).

Quaternary sediments are the youngest sediments recorded in the area that consists of detritus, sands, gravels, pebbles, cobbles, and boulders. They are distributed all over the area and constitute the surficial cover in the main wadis such as Wadi Gasus, Wadi Safaga, Wadi Saqi, and Wadi Abu Aqarib (Figure 3). These originated as a result through the weathering process of the different types of rocks.

## 3. Methodology

The gamma-ray spectrometry method is used in different fields. Initially developed as uranium exploration tool, the application of the method now include geological mapping (Graham and Bonham-carter 1993; Charbonneau et al. 1997), mineral exploration (Lo and Pitcher 1996; Grasty and Shives 1997), soil mapping (Cook et al. 1996; Wilford et al. 1997), and environmental radiation monitoring (Sanderson et al. 1995; Ford et al. 2001). Wilford et al. (1997) demonstrated that airborne gamma-ray spectrometry patterns provided important information for soil, regolith, and geomorphology studies used for land management and mineral exploration

The study area was included in the airborne gamma-ray spectrometric and magnetic survey conducted by Aero-Service Division, Western Geophysical Company of America over a large segment of the central and south Eastern Desert of Egypt. This project aimed essentially to identify and assess the mineral, petroleum and groundwater resources of the region (Aero-Service 1984). The airborne gamma-ray spectrometric survey has a set of parallel traverse flight lines oriented

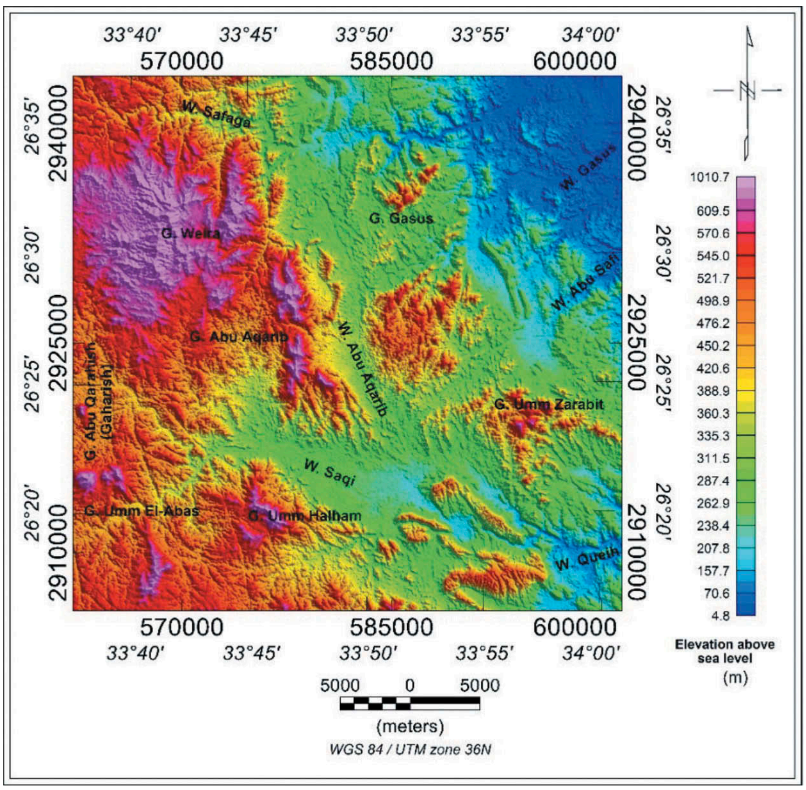


**Figure 2.** Key map showing Elevation above sea level of wadi Queih and wadi Safaga area, Central Eastern Desert, Egypt.

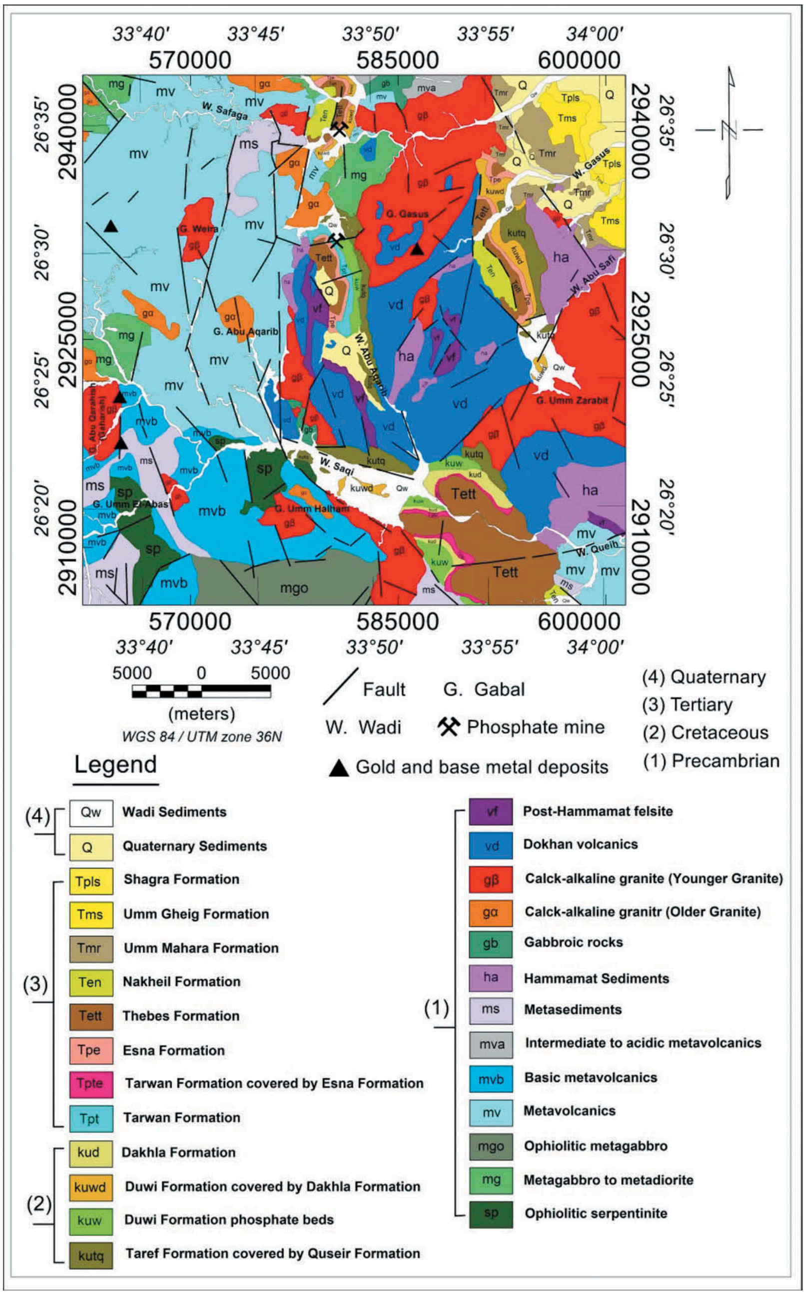


**Figure 3.** Geologic map of Wadi Queih – Wadi Safaga area, Central Eastern Desert, Egypt (Reproduced after Conoco Coral and EGPC, 1987).

northeast-southwest with an azimuth of 45° and 225° from the true north. The flight lines spacing were 1.5 km. The tie lines are oriented in a northwest-southeast direction with an azimuth of 135° and 315° and spacing of 10 km. Survey flying was done at a mean terrain clearance of 120 m with an average aircraft speed ranging from 220 to 315 km/h. The collected spectral gamma-ray measurements were corrected, compiled, and finally displayed as contour maps (Aero-Service 1984). The survey was conducted at a scale of 1:50000 using topographic maps and photomosaic base maps at the same scale (Aero-Service 1984). High-sensitivity 256-channel gamma-ray spectrometer model Hisens AGRS 3000F system was used in measurement by Aero-Service.

The airborne gamma-ray spectrometric data have been processed using OASIS Montaj mapping and processing system (Geosoft 2015). The data are presented as contour maps and they have been subjected to qualitative and quantitative interpretations.

Statistical studies were performed on the airborne spectrometric data in the study area to figure the distribution features of the Total-count (TC), Potassium (K%), Equivalent uranium (eU), Equivalent thorium (eTh), eU/eTh, eTh/K and eU/K. These statistical studies were performed to calculate the minimum, maximum, arithmetic mean (X), standard deviation (S.D.) and coefficient of variability (CV %) which check the normality of each rock unit. (CV % = (S.D./X) *100).

## 4. Results and discussions

### 4.1. Qualitative interpretation

#### 4.1.1. Total-count and radio-elements maps

The total-count (TC), Potassium (K%), Equivalent uranium (eU) and Equivalent thorium (eTh) (Figures 4–7) are characterised by a relatively higher radiometric level in their eastern parts than their western ones. The radioactivity recorded varies widely from one type of rock to the other and some extent between the units of the same rock type. In some cases, the gradients are high enough for delineating the contacts, but sometimes the radioactivity levels of rock units merge into one another, without distinct separations between the different rock types. However, it is possible to distinguish the lithological contacts from the overall changes in the level of radiation.

The examination of the total-count (TC) and three radio-elements (K%, eU, and eTh) maps (Figures 4–7) shows that three distinctive radiometric levels dominate and illustrated as follows:

The low-level has values ranging from 0.1 to 5.4 Ur for total-count, 0.1 to 1% K, less than 1.7 ppm eU and less than 3.3 ppm eTh. These values dominate at the southwestern, western, northern and northeastern parts, associating with the ophiolitic metagabbro, basic metavolcanics, metasediments, serpentines, metavolcanics, metagabbro, metagabbroic rocks, and Umm Gheig Formation.

The moderate-level possesses values varying from 5.4 to 8.5 Ur as a total-count, 1 to 2.3 % K, 1.7 to 4.5 ppm eU and 3.3 to 7 ppm eTh. It is recorded at southeastern, north-central and northeastern parts, associating with Hammamat sediments, alluvium that are derived from granites, older granite and acidic sediments.

The high-level displays values of 8.5 to 23.6 Ur as a total-count, 2.3 to 3.3 %K, 4.5 to 19.1 ppm eU and 7 to 18.9 ppm eTh.Duwi Formation and younger granites at G. Gasus, G. Weira, G. Umm Halham, in the extreme eastern part at G. Umm Zarabit and the extreme wes-tern part of G. Abu Qarahish represent these values.

#### 4.1.2. Radiometric ratio maps

The eU/eTh ratio is beneficial for uranium exploration because it identifies the uranium-enriched areas. eU/eTh contour map (Figure 8) exhibits high eU/eTh ratio zones that reflect increasing of uranium content that dominating over constant thorium content. The eU/eTh values dominate over most geologic units, in the shape of dispersed anomalies scattered in eU/eTh background. eU/eTh ratio contour map shows that the highest values exist over sedimentary rocks, especially over Duwi Formation and small parts of younger granites. The increasing of eU/eTh values over the sedimentary rocks appear to be related to the presence of phosphate and shale beds, which contain a relatively high concentration of U and low to very low values of Th, where U is leachable and mobile when it compared with thorium. The high anomalous values range from 1.2 ppm to more than 2.4 ppm.

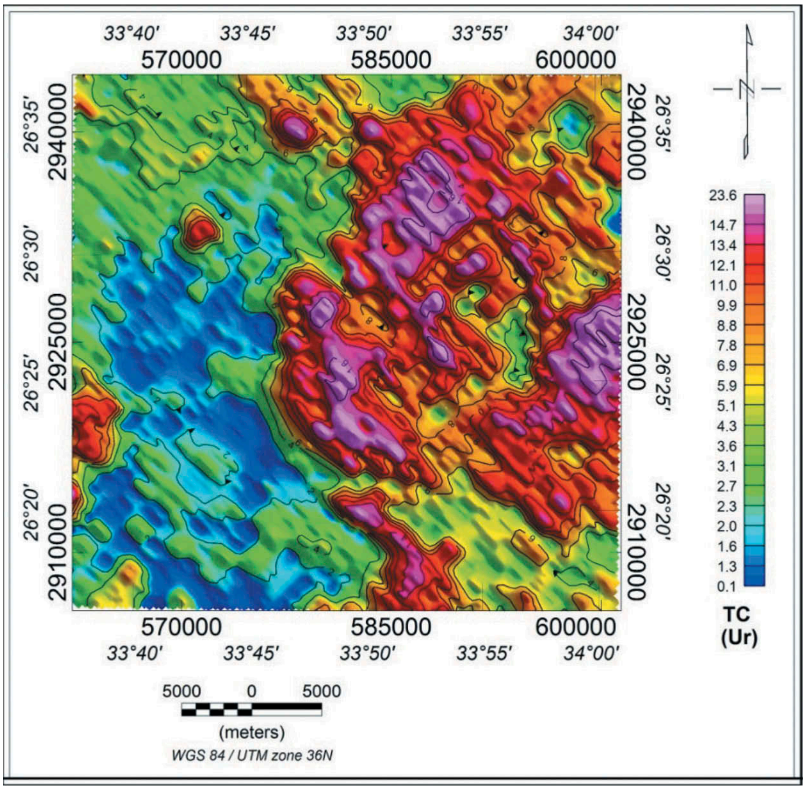


Figure 4. Total-count contour map in Ur, Wadi Queih – Wadi Safaga area, Central Eastern Desert, Egypt. (Aero-Service 1984).

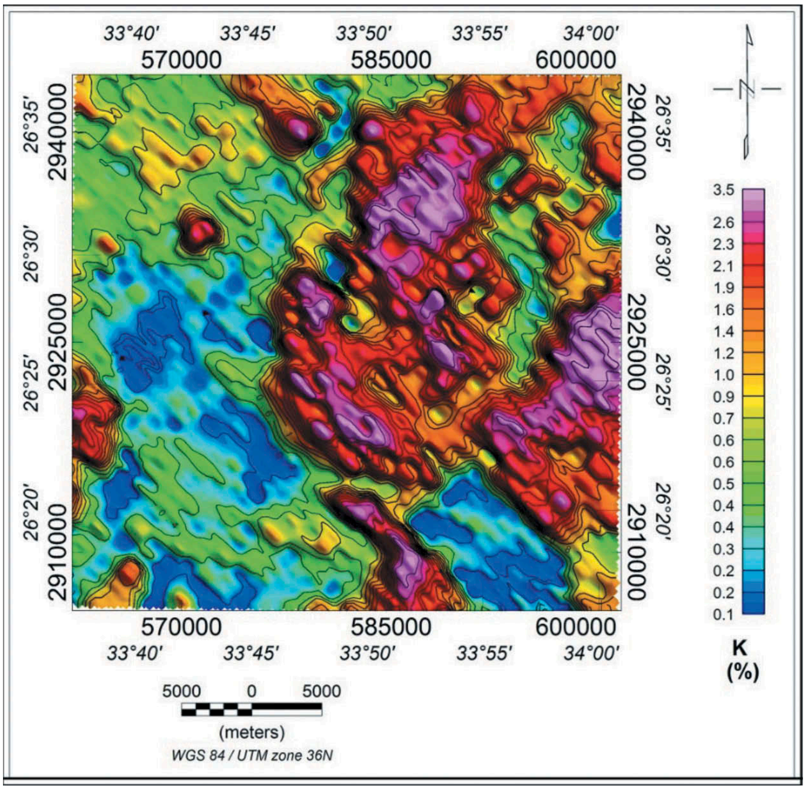


**Figure 5.** Potassium contour map in %, Wadi Queih – Wadi Safaga area, Central Eastern Desert, Egypt. (Aero-Service 1984).

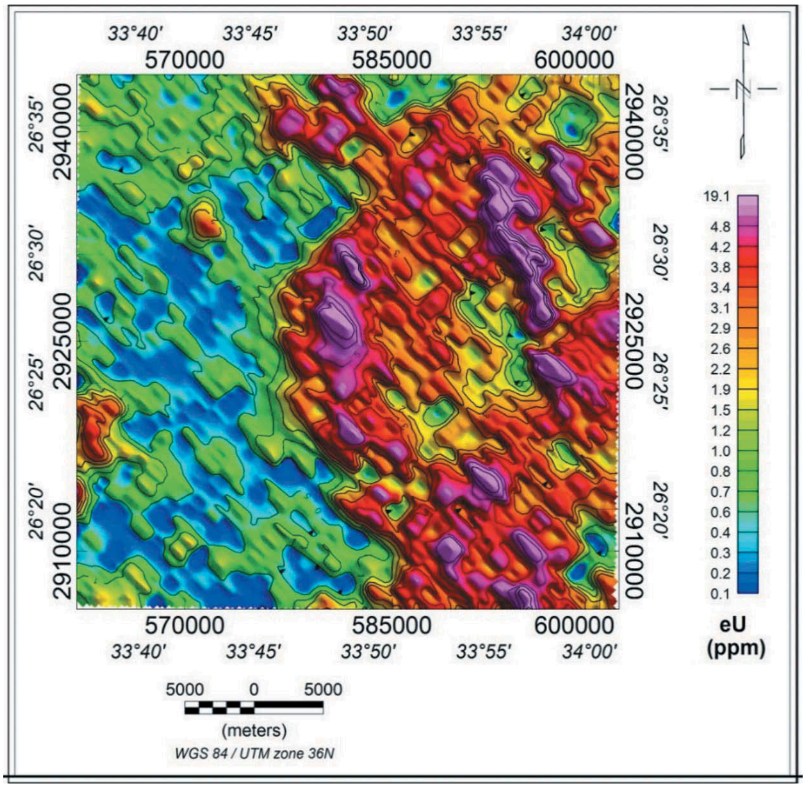


**Figure 6.** Equivalent uranium contour map in ppm, Wadi Queih – Wadi Safaga area, Central Eastern Desert, Egypt. (Aero-Service 1984).

The eU/K ratio contour map (Figure 9) shows that the study area has low eU/K ratio values (<1.6) at the western part, in the form of spots over metavolcanics, metasediments, ophiolitic metagabbro, and granitic rocks. The highest values (> 12) exist over sedimentary rocks, especially Duwi Formation.

The eTh/K ratio contour map (Figure 10) shows three levels of eTh/K ratio. The first level (low) has

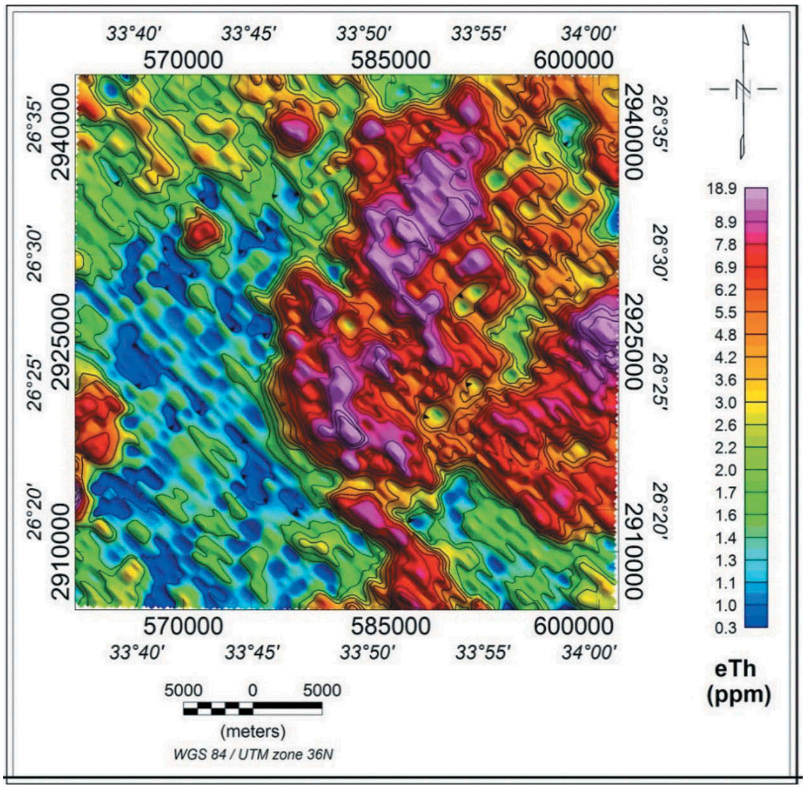


**Figure 7.** Equivalent thorium contour map in ppm, Wadi Queih – Wadi Safaga area, Central Eastern Desert, Egypt. (Aero-Service 1984).

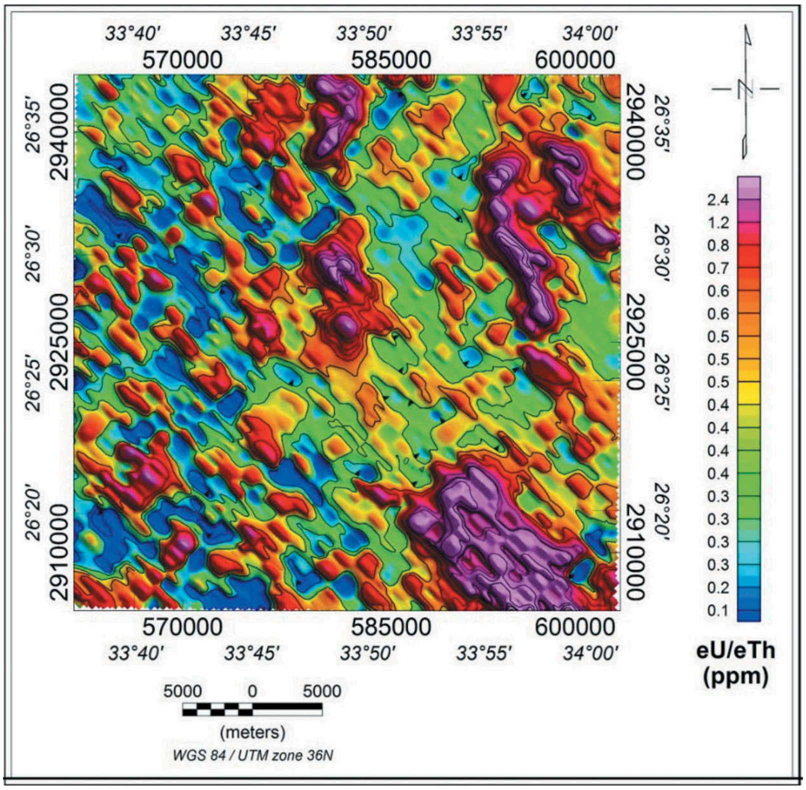


**Figure 8.** eU/eTh ratio contour map, Wadi Queih – Wadi Safaga area, Central Eastern Desert, Egypt.

values ranging from 2.1 to 3.6. It covers a vast area and is associated with the metasediments, metavolcanics group, serpentinites, Dokhan volcanic, gabbroic rocks, and younger granites. The second level (moderate) has values ranging from 3.6 to 5.1 and is spreader all over the area. The third level (high) ranges from 5.1 to < 7.2 eTh/K and dominate over some parts of the sedimentary rocks and older granites all over the study area.

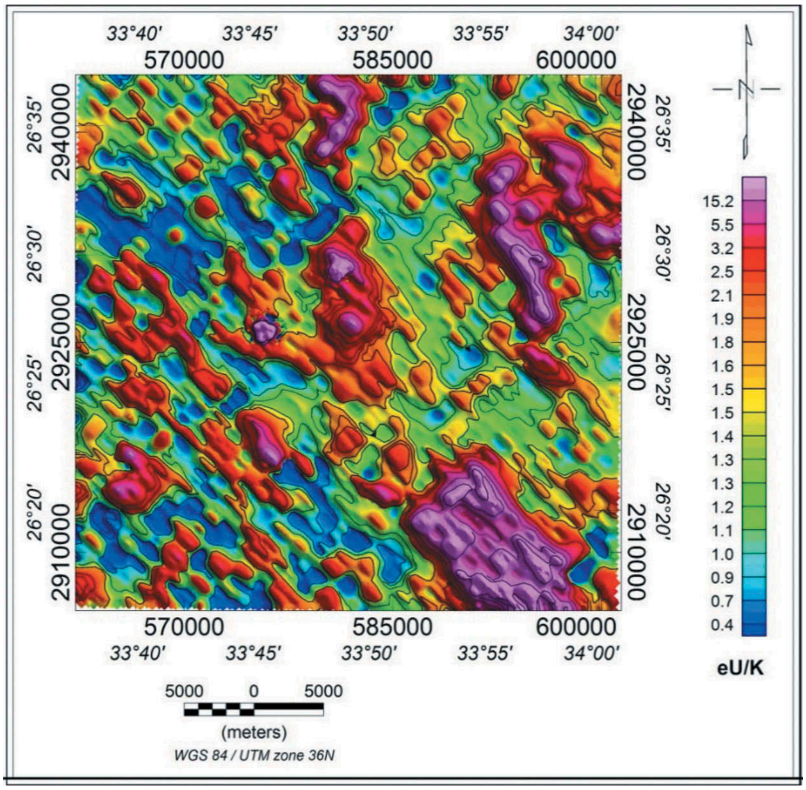


**Figure 9.** eU/K ratio contour map, Wadi Queih – Wadi Safaga area, Central Eastern Desert, Egypt.

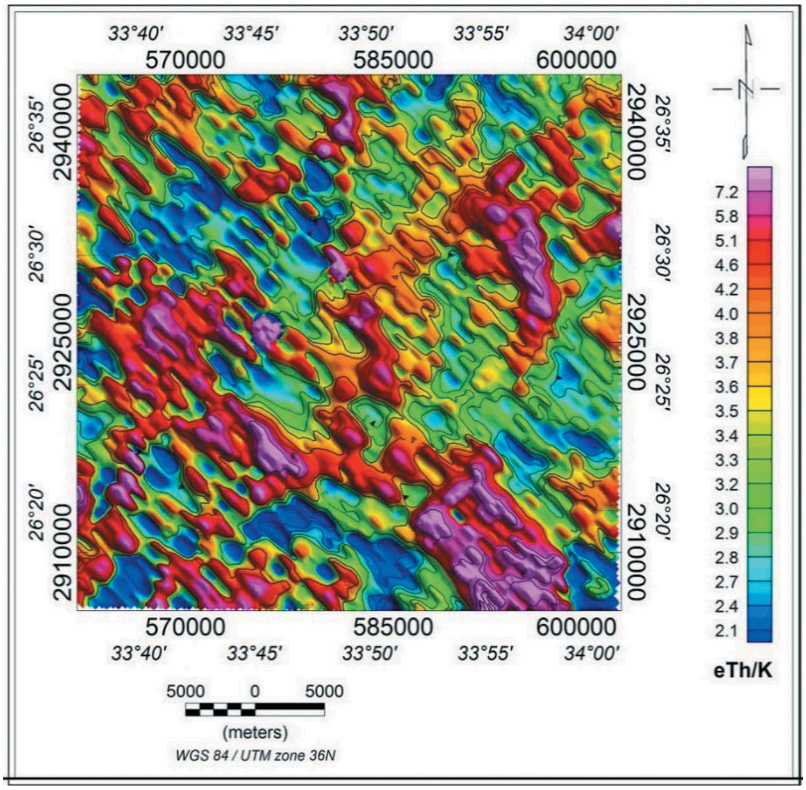


**Figure 10.** eTh/K ratio contour map, Wadi Queih – Wadi Safaga area, Central Eastern Desert, Egypt.

### *4.1.3. Ternary or (composite) image maps*

In this study, two selected ternary composite images, namely: radio-element composite (K, eU, and eTh) and Uranium Composite (eU, eU/eTh, and eU/K) are considered. Composite image map of the radio-elements (Figure 11) mixes the data for eU (in blue), eTh (in green) and K (in red), where blue colour tends to reduce the most reduced signal-to-

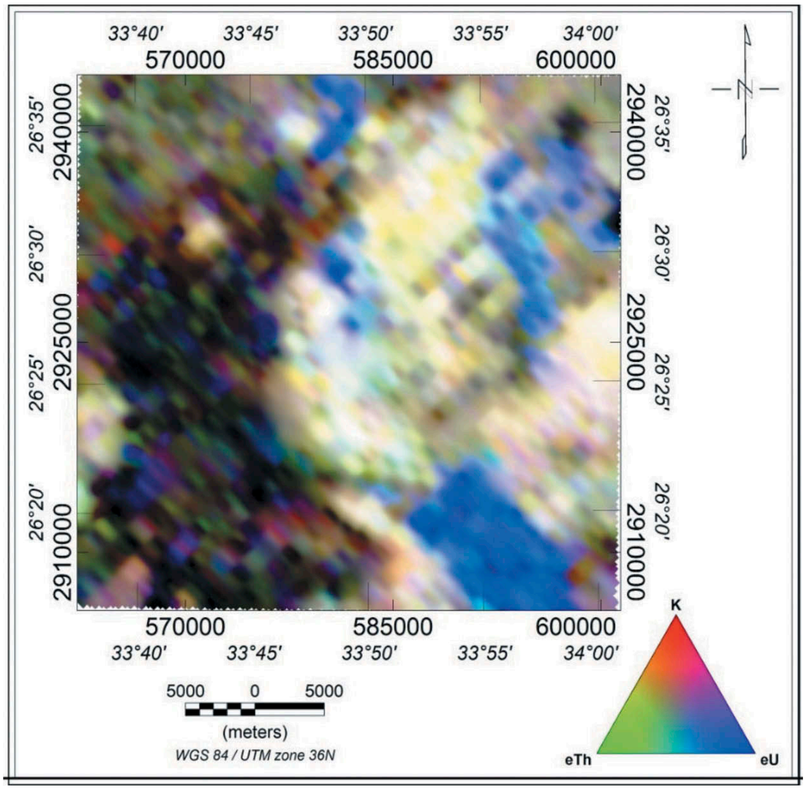


**Figure 11.** Radio-element composite image map of Wadi Queih – Wadi Safaga area, Central Eastern Desert, Egypt.

noise ratio of uranium channel (Milligan and Gunn 1997). This map presents strong spatial correlations with the known geologic units. The metavolcanics and serpentinites appear darker than the surrounding units in the west, indicating lower concentrations in K, eU, and eTh. The high values, observed in a bright colour, are related to younger granites. There are some anomalies, which show strong spatial correlations with the zones of anomalously high eU as blue colour recorder over Duwi phosphate Formation and younger granites. Medium to poor concentrations areas dominates over Hammamat sediments and older granites.

The eU composite image map (Figure 12) provides useful information regarding the identification of anomalous zones of enriched uranium concentration. This map combines eU (in red) with the two ratios eU/eTh (in green) and eU/K (in blue). The anomalous uranium zones are displayed as bright white areas; this is evidence that there is a migration occurred for the uranium, because the amount of uranium is very high in comparison with potassium and thorium, so the ratios eU/K and eU/eTh are very high so they give bright white zones associated with Duwi phosphate Formation. The dark areas (low uranium values) are mainly associated with metavolcanics, metasediments, and older granites. Careful inspection of the uranium composite image map (Figure 12) provides useful information regarding the identification of enriched uranium zones.

### 4.2. *Quantitative interpretation*

Statistical treatments were applied on the airborne gamma-ray spectrometric data in Wadi Queih – Wadi Safaga area to display the distribution features of the TC, K, eU, and eTh. These statistical studies were performed to calculate the minimum, maximum, arithmetic mean (X), standard deviation (S.D.) and coefficient of variability (CV %) which check the normality of each rock unit (CV % = (S.D./X) *100). According to Sarma and Koch (1980), if the (CV %) of a specific rock unit is less than 100%, the unit tends to exhibit a normal distribution. The data treated. Statistically, Table 1 shows the results of this analysis.

#### 4.2.1. *Precambrian basement rocks*

The coefficient of variability (CV%) less than 100% characterises most of the Pre-Cambrian basement rocks for all the radiometric parameters (TC., K%, eU, and eTh). Therefore, the rock units tend to normality in their distribution. The ophiolitic serpentinite rocks display the highest values of CV% for the radiometric parameters (TC, K%, eU, and eTh) with values of 79.27, 94.59, 71.43, and 46.03, respectively. Accordingly, they have the lowest degree of homogeneity in the basement rocks of the study area. Meanwhile, Post-Hammamat felsite rock units possess the lowest values of CV% for the TC, K%, eU and eTh

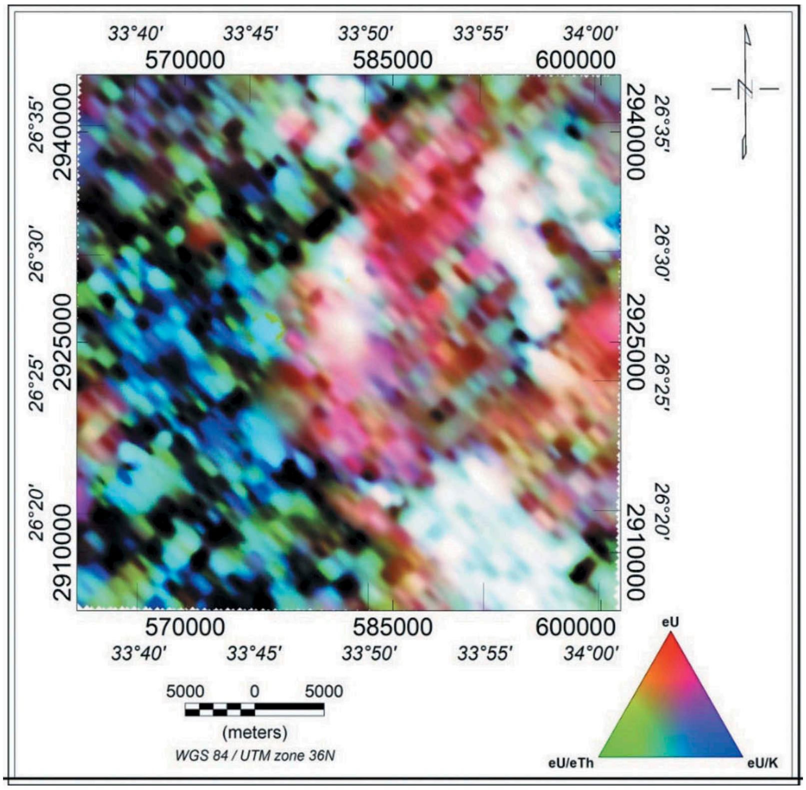


**Figure 12.** Equivalent uranium composite image map of Wadi Queih – Wadi Safaga area, Central Eastern Desert, Egypt.

with values of 25.88, 24.24, 33.72 and 26.95 respectively, which reflect that these rocks have the highest degree of homogeneity. Table 1 shows that the wide range of eU values associated with Hammamat sediments (0.01 to 14.97 ppm) and younger granites (0.01 to 10.3 ppm).

#### 4.2.2. Sedimentary rocks

*4.2.2.1. Cretaceous rocks.* The coefficient of variability (CV %) less than 100% characterises the Cretaceous sedimentary rocks. So, the rock units tend to normality in their distribution except for Thebes Formation (111.32% in K). The highest uranium concentrations exists over Taref Formation with equivalent uranium (eU) values that ranged from 0.01 to 19.01 ppm, a mean of 5.76 ppm and coefficient of variability 67.36%, the potassium (K) values range from 0.16 to 2.57% with a mean of 1.1% and coefficient of variability of 56.36%, and the equivalent thorium (eTh) values differ from 1.53 to 12.19 ppm with a mean of 5.21 ppm and coefficient of variability of 41.45%. These relative higher values may be due to migration of the radioelements from the surrounding rock units. Statistical analysis clearly shows that the Duwi Formation has high radiometric values with equivalent uranium (eU) values ranging from 1.33 to 14.98ppm and a mean of 4.90 ppm, coefficient of variability 53.88%, the potassium (K) values range from 1.3 to 2.86% with a mean of 1.27% and coefficient of variability of 51.97%, and the equivalent thorium (eTh) values are differing from 1.4 to 7.85 ppm with a mean of 4.7 ppm and coefficient of variability of 35.74%.

#### 4.2.3. Tertiary rocks

The coefficient of variability (CV %) less than 100%, which reflects that the rock units tend to normality in their distribution. The high uranium concentrations of these rocks are recorded over Umm Mahara Formation varying in the equivalent uranium (eU) values ranging from 0.74 to 14.54 ppm with a mean of 3.72 ppm and coefficient of variability 56.45%, the potassium (K) values range from 0.3 to 2.78% with a mean of 1.24% and coefficient of variability of 37.9%, and the equivalent thorium (eTh) values are varying from 1.29 to 8.38 ppm with a mean of 4.13 ppm and coefficient of variability of 29.54%.

#### 4.2.4. Quaternary rocks

The coefficient of variability of Quaternary sediments (CV %) is less than 100%, which reveals the rock units tend to normality in their distribution. The radioactivity of Wadi sediments increases in the direction of both sides of the younger granites. The outcome of washing-out materials from the rock units that are surrounding them have sharper radiometric anomalies to the mouth of the wadi. They have equivalent uranium (eU) values ranging from 0.01to 19.07 ppm with a mean of 2.35 ppm and coefficient of variability 97.02%, the potassium (K) values range from 0.05 to 2.92% with a mean of 1.01% and coefficient of variability of 68.32%,

**Table 1.** Summary of the statistical treatments of gamma-ray spectrometric data for the Precambrian basement rock units of Wadi Queih – Wadi Safaga area, Central Eastern Desert, Egypt.

| Rock unit | statistical parameter | TC | K | eU | eTh | Rock unit | statistical parameter | TC | K | eU | eTh |
|---|---|---|---|---|---|---|---|---|---|---|---|
| Ophiolitic serpentinite | Min | 0.3 | 0.03 | 0.01 | 0.32 | Duwi Formation (225) | Min | 4.4 | 0.13 | 1.33 | 1.4 |
| (517) | Max | 7.74 | 1.73 | 1.9 | 3.2 | | Max | 21.39 | 2.86 | 14.89 | 7.85 |
| | X | 1.93 | 0.37 | 0.56 | 1.26 | | X | 9.76 | 1.27 | 4.9 | 4.7 |
| | S.D. | 1.53 | 0.35 | 0.4 | 0.58 | | S.D. | 3.13 | 0.66 | 2.64 | 1.68 |
| | CV% | 79.27 | 94.59 | 71.43 | 46.03 | | CV% | 32.07 | 51.97 | 53.88 | 35.74 |
| Metagabbro to metadiorite | Min | 0.94 | 0.12 | 0.04 | 0.68 | Duwi Formation covered by | Min | 3.14 | 0.04 | 0.75 | 1.29 |
| (662) | Max | 16.14 | 2.92 | 3.98 | 10.16 | Dakhla Formation (231) | Max | 17.49 | 2.61 | 15.08 | 10.95 |
| | X | 4.62 | 0.83 | 1.15 | 2.8 | | X | 9.6 | 0.86 | 6.08 | 3.94 |
| | S.D. | 3.27 | 0.58 | 0.9 | 1.91 | | S.D. | 3.59 | 0.63 | 3.22 | 2.19 |
| | CV% | 70.78 | 69.88 | 78.26 | 68.21 | | CV% | 37.4 | 73.25 | 52.96 | 55.58 |
| Ophiolitic metagabbro | Min | 0.45 | 0.1 | 0.01 | 0.61 | Dakhla Formation (140) | Min | 4.08 | 0.1 | 1.06 | 1.11 |
| (645) | Max | 8.11 | 1.42 | 2.92 | 5.66 | | Max | 12.82 | 2.12 | 9.83 | 7.73 |
| | X | 2.11 | 0.38 | 0.57 | 1.51 | | X | 7.1 | 0.62 | 4.51 | 2.97 |
| | S.D. | 1.23 | 0.2 | 0.45 | 0.69 | | S.D. | 2.24 | 0.54 | 2.04 | 1.64 |
| | CV% | 58.29 | 52.63 | 78.95 | 45.69 | | CV% | 31.55 | 87.1 | 45.23 | 55.22 |
| Metavolcanics (4845) | Min | 0.03 | 0.01 | 0.01 | 0.34 | Tarwan Formation (79) | Min | 1.95 | 0.01 | 0.01 | 0.86 |
| | Max | 15.79 | 2.89 | 5.45 | 10.14 | | Max | 14.98 | 2.4 | 9.09 | 8.39 |
| | X | 2.84 | 0.53 | 0.77 | 1.79 | | X | 7.59 | 1.07 | 4.61 | 3.86 |
| | S.D. | 1.55 | 0.29 | 0.64 | 0.84 | | S.D. | 4.21 | 0.7 | 2.89 | 2.32 |
| | CV% | 54.58 | 54.72 | 49.28 | 46.93 | | CV% | 55.47 | 65.42 | 62.69 | 60.1 |
| Basic Metavolcanics (1760) | Min | 0.37 | 0.06 | 0.01 | 0.29 | Tarwan Formation covered by | Min | 4.02 | 0.03 | 1 | 1.07 |
| | Max | 11.17 | 1.83 | 2.75 | 7.96 | Esna Formation (111) | Max | 14 | 2.23 | 12.45 | 8.26 |
| | X | 2.32 | 0.45 | 0.59 | 1.55 | | X | 6.95 | 0.57 | 4.64 | 2.8 |
| | S.D. | 1.15 | 0.22 | 0.38 | 0.76 | | S.D. | 2.7 | 0.53 | 2.28 | 1.46 |
| | CV% | 27 | 48.89 | 64.41 | 49.03 | | CV% | 38.85 | 93 | 49.14 | 52.14 |
| Intermediate to acidic | Min | 2.13 | 0.43 | 0.29 | 1.23 | Esna Formation (180) | Min | 2.34 | 0.01 | 0.28 | 0.8 |
| metavolcanics (81) | Max | 6.14 | 1.09 | 3.31 | 3.55 | | Max | 18.43 | 2.86 | 13 | 10.97 |
| | X | 3.63 | 0.69 | 0.85 | 2.01 | | X | 8.9 | 1.02 | 4.94 | 4.22 |
| | S.D. | 0.98 | 0.16 | 0.52 | 0.65 | | S.D. | 4.26 | 0.77 | 2.55 | 2.62 |
| | CV% | 27 | 23.19 | 61.18 | 32.34 | | CV% | 47.86 | 75.49 | 51.62 | 62.08 |
| Metasediments (845) | Min | 0.88 | 0.05 | 0.05 | 0.33 | Thebes Formation (1149) | Min | 2.42 | 0.03 | 0.76 | 0.72 |
| | Max | 14.88 | 2.48 | 5.25 | 13.27 | | Max | 20.53 | 3.27 | 12.61 | 12.53 |
| | X | 3.51 | 0.62 | 1.15 | 2.06 | | X | 6.32 | 0.53 | 4.3 | 2.61 |
| | S.D. | 2.19 | 0.36 | 0.92 | 1.62 | | S.D. | 2.67 | 0.59 | 1.38 | 2.13 |
| | CV% | 62.39 | 56.06 | 80 | 78.64 | | CV% | 42.25 | 111.32 | 32.1 | 81.61 |
| Hammamat Sediments | Min | 1.44 | 0.19 | 0.01 | 1.16 | Nakheil Formation (198) | Min | 4.1 | 0.11 | 1.28 | 1.24 |
| (1044) | Max | 15.82 | 2.81 | 14.97 | 10.49 | | Max | 17.68 | 2.96 | 4.91 | 12.47 |
| | X | 9.21 | 1.43 | 3.23 | 5.24 | | X | 9.79 | 1.54 | 3.27 | 5.85 |
| | S.D. | 2.57 | 0.54 | 2.35 | 1.66 | | S.D. | 3.51 | 0.72 | 0.86 | 2.93 |
| | CV% | 27.9 | 37.76 | 72.75 | 31.68 | | CV% | 35.85 | 46.75 | 26.3 | 50.08 |
| Gabbroic rocks (110) | Min | 2.22 | 0.48 | 0.12 | 1.32 | Umm Mahara Formation (406) | Min | 2.29 | 0.3 | 0.74 | 1.29 |
| | Max | 12.19 | 2.22 | 4.38 | 7.71 | | Max | 18.19 | 2.78 | 14.54 | 8.38 |
| | X | 5.21 | 0.91 | 1.31 | 3.12 | | X | 8.65 | 1.24 | 3.72 | 4.13 |
| | S.D. | 2.34 | 0.43 | 0.74 | 1.35 | | S.D. | 2.4 | 0.47 | 2.1 | 1.22 |
| | CV% | 44.91 | 47.25 | 56.49 | 43.27 | | CV% | 27.74 | 37.9 | 56.45 | 29.54 |
| Calck-alkaline granite (Older | Min | 0.75 | 0.14 | 0.01 | 0.55 | Umm Gheig Formation (261) | Min | 0.91 | 0.05 | 0.1 | 0.91 |
| Granite) | Max | 9.33 | 1.55 | 2.75 | 6.93 | | Max | 11.84 | 1.87 | 11.09 | 5.88 |
| (508) | X | 3.33 | 0.63 | 0.85 | 1.96 | | X | 5.56 | 0.75 | 2.47 | 2.73 |
| | S.D. | 2.04 | 0.4 | 0.55 | 1.01 | | S.D. | 2.88 | 0.44 | 2.26 | 1.25 |
| | CV% | 61.26 | 63.49 | 64.7 | 51.53 | | CV% | 51.8 | 58.66 | 91.5 | 45.79 |
| Calck-alkaline granite | Min | 1.15 | 0.21 | 0.01 | 0.46 | Shagra Formation (169) | Min | 1.89 | 0.32 | 0.25 | 1.37 |
| (Younger Granite) | Max | 20.02 | 3.45 | 10.3 | 12.89 | | Max | 11.6 | 1.99 | 3.84 | 6.97 |
| (3793) | X | 11.73 | 2.15 | 2.91 | 6.94 | | X | 7.39 | 1.3 | 2.04 | 4.23 |
| | S.D. | 4.1 | 0.74 | 1.2 | 2.74 | | S.D. | 2.66 | 0.45 | 0.86 | 1.57 |
| | CV% | 34.95 | 34.42 | 41.24 | 39.48 | | CV% | 36 | 34.61 | 42.16 | 37.11 |
| Dokhan volcanics (2790) | Min | 1.58 | 0.21 | 0.39 | 1.38 | Quaternary Sediments (723) | Min | 2.9 | 0.35 | 1.11 | 1.68 |
| | Max | 23.55 | 3.49 | 8.2 | 18.78 | | Max | 19.04 | 3.08 | 13.46 | 12.61 |
| | X | 10.63 | 1.85 | 2.85 | 6.58 | | X | 9.72 | 1.49 | 3.63 | 5.2 |
| | S.D. | 3.64 | 0.64 | 1.11 | 2.67 | | S.D. | 3.4 | 0.61 | 1.85 | 2.21 |
| | CV% | 34.24 | 34.59 | 38.95 | 40.58 | | CV% | 34.98 | 40.94 | 50.96 | 42.5 |
| Post-Hammamat felsite | Min | 3.14 | 0.59 | 0.5 | 2.41 | Wadi Sediments (1473) | Min | 0.59 | 0.05 | 0.01 | 0.62 |
| (313) | Max | 21.06 | 3.3 | 7.51 | 15.23 | | Max | 19.65 | 2.92 | 19.07 | 12.57 |
| | X | 13.06 | 2.31 | 3.41 | 7.94 | | X | 6.44 | 1.01 | 2.35 | 3.6 |
| | S.D. | 3.38 | 0.56 | 1.15 | 2.14 | | S.D. | 4.16 | 0.69 | 2.28 | 2.18 |
| | CV% | 25.88 | 24.24 | 33.72 | 26.95 | | CV% | 64.6 | 68.32 | 97.02 | 60.55 |
| Taref Formation covered by | Min | 1.6 | 0.16 | 0.01 | 1.53 | | | | | | |
| Quseir Formation | Max | 21.95 | 2.57 | 19.01 | 12.19 | | | | | | |
| (536) | X | 10.46 | 1.1 | 5.76 | 5.21 | | | | | | |
| | S.D. | 3.61 | 0.62 | 3.88 | 2.16 | | | | | | |
| | CV% | 34.51 | 56.36 | 67.36 | 41.45 | | | | | | |

Min = minimum, Max = maximum, X = mean, S.D. = Standard Deviation, CV % = Coefficient of Variability in % and (517) = Number of readings over every lithologic unit, (TC) = Total-count, (K%) = Potassium, (eU) = Equivalent uranium, (eTh) = Equivalent thorium.

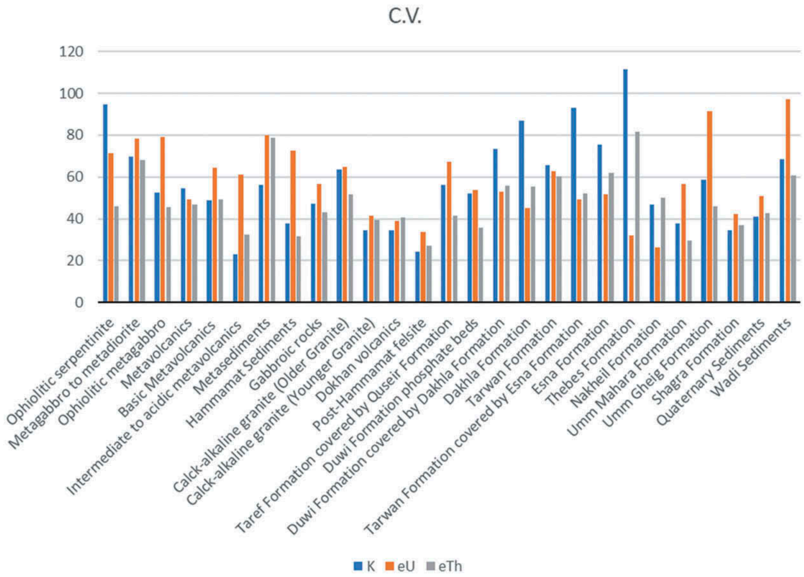


**Figure 13.** Vertical bar charts showing the calculated coefficients of variability (CV) of the K, eU and eTh for the different rock units of Wadi Queih – Wadi Safaga area, Central Eastern Desert, Egypt.

and the equivalent thorium (eTh) values vary from 0.62 to 12.57 ppm with a mean of 3.60 ppm and Coefficient of Variability of 60.55%.

The (CV %) of the gamma-ray spectrometric variables (eU, eTh, and K) of all rock units in the study area has been calculated and listed in the Table 1 and illustrated as a bar graph (Figure 13). The examination of the table and the bar graph for the study area shows that all rock units show a normal distribution of the three radiometric variables, except for the potassium in the Thebes Formation which has a (CV %) value higher than 100.

## 5. Structural lineaments interpretation

A set of rose diagrams, representing the azimuth distributions of length and number percentages of lineaments within the study area, are constructed. These rose diagrams illustrate the trends of the significant structural lineament of the study area deduced from the surface geology, TC, K%, eU, and eTh is shown in Figure 14.

The significant faults systems were recognised very obviously on the geologic map (Figure 14(a)) as linear segments of stream valleys or other geomorphological alignments. As a conclusion, the predominant trends, arranged according to their cumulative number and length percentages, taking the N-S, NNW-SSE, NNE-SSW directions. The diagram also shows the presence of other minor trends in all directions.

The correlation between radio-spectrometric rose diagrams of the TC, K%, eU, and eTh (Figure 14(b–e)) generally show the same trends and confirms each other. The structural features trend mainly in the NW-SE and NE-SW directions. Therefore, these trends are considered the most significant trends in the study area from the radiometric point of view.

Finally, from the close inspection of the all radiometric presented maps (Figures 4–14), it can deduce that, the highest uraniferous zones are associated with the younger granitic rocks and Duwi Formation. These zones are considered exploration targets for ground geological, geophysical and geochemical follow-up investigations. In addition, the NW-SE, NE-SW and the intersections of these trends are the most important trends for uranium exploration in the area under investigation.

## 6. Conclusions

Analysis of the airborne gamma-ray spectrometric data of the study area revealed the following concluding remarks:

(1) The high radiometric values dominate over the outcropping younger granites and Duwi Formation. Meanwhile, the lowest values exist over ophiolitic metagabbro, basic metavolcanics, metasediments, serpentinites, and Umm Gheig Formation.
(2) A clear high anomalous zones of eU dominate on the composite eU image map as bright white area. These zones are considered exploration targets for ground geophysical and geochemical follow-up investigations.
(3) The statistically results showed that the study area has a wide range of radioactivity ranging between 0.1 to 23.6 Ur for TC, 0.1 to 3.3% for K, 0.01 to 19.1ppm for eU and 0.29 to 18.9ppm eTh.

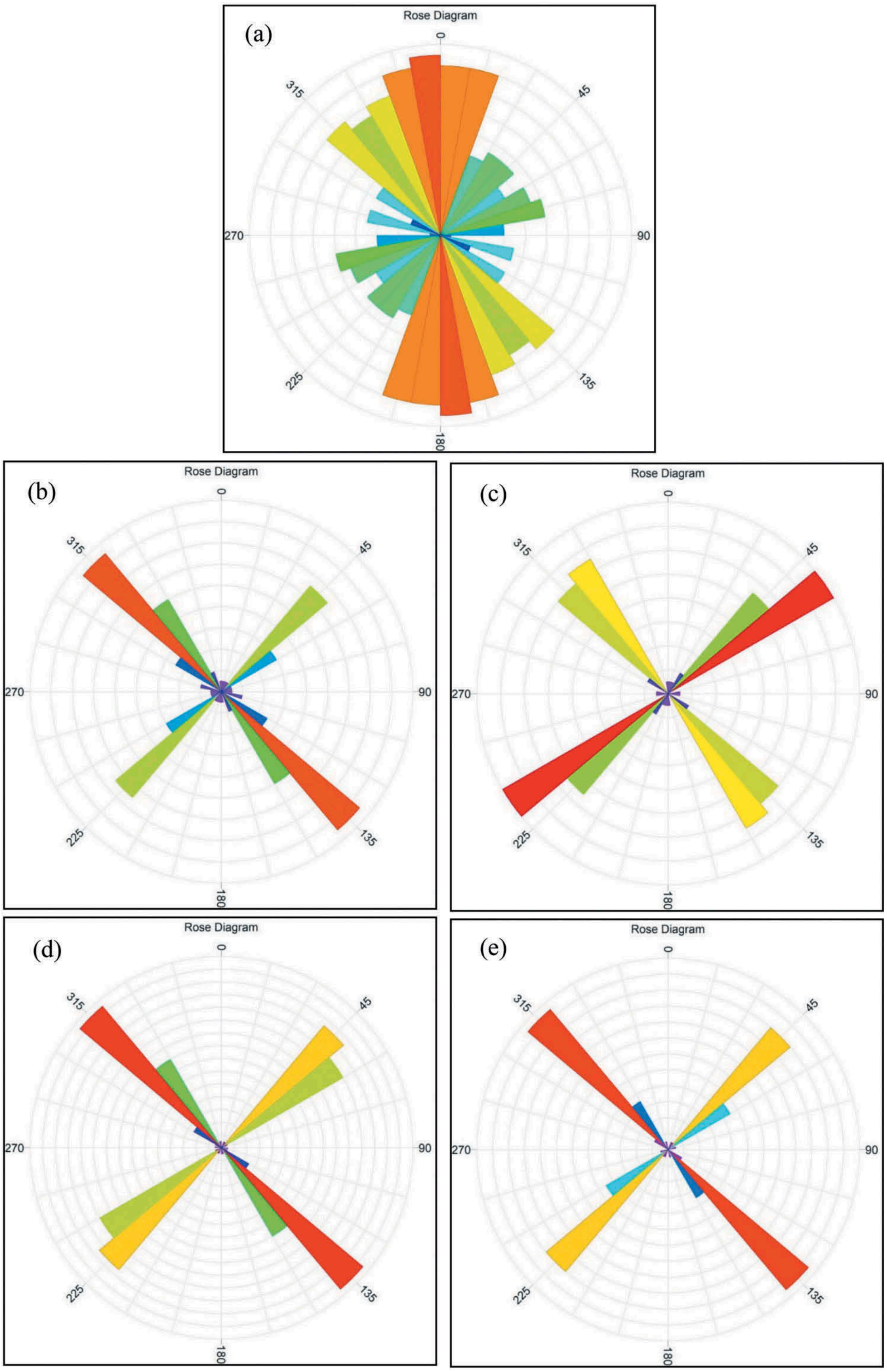


Figure 14. Rose diagrams showing the main structural lineaments that deduced from (a) geologic, (b) TC, (c) K, (d) eU and (e) eTh maps of Wadi Queih – Wadi Safaga area, Central Eastern Desert, Egypt.

(4) All rock units in the study area have a normal distribution for the three radio-elements, except for potassium in Thebes Formation, where these rock units exhibited CV values of less than 100%.

(5) The most important trends in the study area are NW-SE and NE-SW, which coincide to a great extent with the structural trend dominate in the study area.

## Disclosure statement

No potential conflict of interest was reported by the authors.

## References

Aero-Service. 1984. Final report on airborne magnetic and radiation survey in Eastern Desert, Egypt. Work completed for the Egyptian General Petroleum Corporation (EGPC). Six volumes, Aero -Service. Houston (TX).

Akaad MK, El-Ramly MF. 1960b. Geological history and classification of the basement rocks of the Central-Eastern Desert of Egypt. Geological Survey of Egypt, Cairo, Paper No. 9; p. 24.

Ammar AA, Abdel Hadi HM, Soliman SA, Sadek HS. 1988. Aerial radioactivity of phosphates in the Western Central Eastern Desert of Egypt. JKAU Earth Sci. 1:181–203.

Charbonneau BW, Holman PB, Hetu RJ. 1997. Airborne gamma spectrometer magnetic-VLF survey of north-eastern Alberta. In Exploring for minerals in Alberta: geological Survey of Canada Geoscience contributions, edited by MacQueen, Canada-Alberta agreement on mineral development. Geoll Surv Canada Bull. 500:107–132.

Conoco Coral Corporation and the Egyptian General Petroleum Corporation (EGPC). 1987. Geological map of Egypt, Scale 1: 500000 –NG 36 SE- Quseir.

Cook SE, Corner RJ, Groves PR, Grealish GJ. 1996. Use of airborne gamma radiometric data for soil mapping. Aust J Soil Res. 34:183–190.

Darnely AG, Ford KL 1989. Regional airborne gamma -ray surveys, a review. In: Garland GD, edited by. Proceedings of Exploration, 87; Third Decennial Inter –national Conference on Geophysical and Geochemical Exploration for Minerals and Groundwater; Ontario, Canada: Geological Survey of Canada, Special V.3. p. 229–240.

El Qassas RAY. 2018. Application of airborne spectral gamma-ray data for delineating surface distribution of heat production at Gebel El Bakriyah – wadi El Batur area, Central Eastern Desert, Egypt. Egs J. 15 (1):187–198.

El-Ramly MF. 1972. A new geological map for the basement rocks in the Eastern and South-Eastern deserts of Egypt, scale 1: 1,000,000. Ann Geol Surv Egypt. 2(1):11.

Ford KL, Savard M, Dessau J-C, Pellerin E. 2001. The role of gamma-ray spectrometry in radonrisk evaluation: A case history from Oka, Quebec. Geosci Can. 28:2.

Geosoft. 2015. Oasis Montaj 8.3.3 mapping and processing system. Geosoft Inc.

Graham DF, Bonham-carter GF. 1993. Airborne radiometric data: a tool for reconnaissance geological mapping using a GIS. Photogramm Eng Remote Sen. 58:1243–1249.

Grasty RL, Shives RBK. 1997. Applications of gamma ray spectrometry to mineral exploration and geological mapping. Workshop presented at Exploration 97: Fourth Decennial Conference on Mineral Exploration.

Hume WF. 1937. The fundamental Pre-Cambrian rocks of Egypt and the Sudan, their distribution, age and character, the minerals of economic value associated with the intrusive Precambrian igneous rocks. Geology of Egypt. 2, Part 3, Survey of Egypt; Cairo: Government Press, p. 689–990.

Ibrahim MM. 1941. The igneous activities. Privately printed. Cairo: Al Etemad Press.

International Atomic Energy Agency (IAEA). 2003. Guidelines for Radioelement Mapping Using Gamma-ray Spectrometry Data. Technical Reports Series No., IAEATECDOC-1363. Vienna (Austria); p. 179.

Lo BH, Pitcher DH. 1996. A case history on the use of regional aeromagnetic and radiometric data sets for lode gold exploration in Ghana. Annual Meeting Expanded Abstracts; Society of Exploration Geophysicists, p. 592–595.

Milligan PR, Gunn PJ. 1997. Enhancements and presentation of airborne geophysical data. ASGO J Aust Geol Geophys. 17(31–38):2.

Sadek HS. 1972. Regional aeroradiometric survey of East Luxor area and its relation to stratigraphy and regional geology [M.Sc. thesis] Faculty of Science Cairo University, p. 131.

Salahel-Din K. 2009. Estimation of heat generation by radioactive decay of some phosphate rocks in Egypt. Appli Radiat Isot. 67:2033–2036.

Salman AB. 1974. Structures and radioactivity of some phosphate deposits, East Luxor area, Eastern Desert Egypt [Ph. D. thesis]. Faculty of Science Ain Shams University, p. 322.

Sanderson DCW, Allyson JD, Tyler AN, Scott EM. 1995. Environmental applications of airborne gamma ray spectrometry. Application of Uranium Exploration Data and Techniques in Environmental Studies, IAEATECDOC- 827; Vienna: IAEA, p. 71–79.

Sarma DD, Koch GS. 1980. A statistical analysis of exploration geochemical data for uranium. Math Geol. 12 (2):99–114.

Wilford JR, Bierwirth PN, Craig MA. 1997. Application of airborne gamma-ray spectrometry in soil/regolith mapping and applied geomorphology. ASGO J Aust Geol Geophys. 17,:201–216.